Remote Sensing and Modeling of Coherent Structures in River and Estuarine Flows

Andrew T. Jessup
Applied Physics Laboratory
University of Washington
1013 NE 40th St.
Seattle, WA 98105-6698
phone: (206) 685-2609 fax: (206) 543-6785 email: jessup@apl.washington.edu

Robert L. Street
Department of Civil and Environmental Engineering
Stanford University, Stanford, CA 94305-4020
phone: (650) 723-4969 fax: (650) 725-39720 e-mail: street@stanford.edu

Stephen G. Monismith
Department of Civil and Environmental Engineering
Stanford University, Stanford, CA 94305-4020
phone: (650) 723-4764 fax: (650) 725-9720 email: monismith@stanford.edu

Alexander R. Horner-Devine
Department of Civil and Environmental Engineering
University of Washington
Seattle, WA 98195-2700
Phone: (206) 685-3032 fax: (206) 685-9185 email: arhd@u.washington.edu

Award Number: N00014-05-1-0485

LONG-TERM GOALS

The long-term goals of this research are to combine state-of-the-art remote sensing and *in situ* measurements with advanced numerical modeling (a) to characterize coherent structures in river and estuarine flows and (b) to determine the extent to which their remotely sensed signatures can be used to initialize and guide predictive models.

OBJECTIVES

Coherent structures are generated by the interaction of the flow with bathymetric and coastline features. These coherent structures produce surface signatures that can be detected and quantified using remote sensing techniques. Furthermore, a number of relationships between coherent structures and flow characteristics have been suggested that have the potential to allow flow parameters (e.g. mean velocity, bottom roughness, shear, and turbidity) to be inferred from remote measurements. The objectives are to test the following four hypotheses:

1. Flow parameters can be inferred from remotely sensed signatures of coherent structures.
2. Numerical models can be constrained with these inferred parameters.

Report Documentation Page

Form Approved
OMB No. 0704-0188

1. REPORT DATE	2. REPORT TYPE	3. DATES COVERED
30 SEP 2006		**00-00-2006 to 00-00-2006**

4. TITLE AND SUBTITLE	5a. CONTRACT NUMBER
Remote Sensing and Modeling of Coherent Structures in River and Estuarine Flows	5b. GRANT NUMBER
	5c. PROGRAM ELEMENT NUMBER
6. AUTHOR(S)	5d. PROJECT NUMBER
	5e. TASK NUMBER
	5f. WORK UNIT NUMBER
7. PERFORMING ORGANIZATION NAME(S) AND ADDRESS(ES) **University of Washington,Applied Physics Laboratory,1013 N.E. 40th St.,Seattle,WA,98105**	8. PERFORMING ORGANIZATION REPORT NUMBER
9. SPONSORING/MONITORING AGENCY NAME(S) AND ADDRESS(ES)	10. SPONSOR/MONITOR'S ACRONYM(S)
	11. SPONSOR/MONITOR'S REPORT NUMBER(S)

12. DISTRIBUTION/AVAILABILITY STATEMENT
Approved for public release; distribution unlimited

13. SUPPLEMENTARY NOTES

14. ABSTRACT

15. SUBJECT TERMS

16. SECURITY CLASSIFICATION OF:			17. LIMITATION OF ABSTRACT	18. NUMBER OF PAGES	19a. NAME OF RESPONSIBLE PERSON
a. REPORT	b. ABSTRACT	c. THIS PAGE			
unclassified	**unclassified**	**unclassified**	**Same as Report (SAR)**	**22**	

3. The effect of stratification on the strength of coherent structures can be used to detect the presence or absence of stratification and the location of the fresh/salt water interface.

4. Numerical and field experiments can be used together to predict, interpret, characterize, and understand coherent structures.

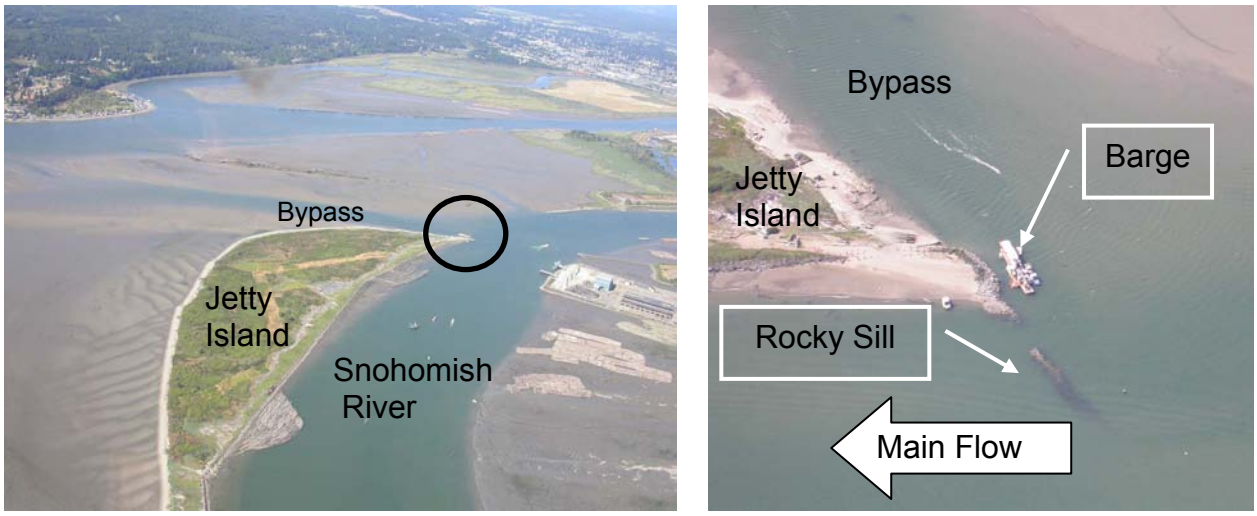

Figure 1. Aerial photographs of the Snohomish River showing the location of the study area at the north tip of Jetty Island. The photograph on the right shows the location of the instrument barge and rocky sill at the north tip of Jetty Island.

APPROACH

The key to this project is an interactive process that blends sophisticated remote sensing, in-situ measurements, and numerical simulation. Our approach is to conduct closely coupled field and numerical model experiments to test the hypotheses listed above. The plan includes two major field experiments with both *in situ* and remote sensing measurements – the first occurred in Year 2 (this reporting period, see below) and the second is planned for Year 4. A preliminary experiment was conducted in Year 1 to aid in the design of the major field efforts. The research involves four main areas - (1) *in situ* measurements, (2) remote sensing, (3) modeling, and (4) physics and classification of coherent structures. The *in situ* field measurements will be used to characterize the overall flow field to investigate the generation of coherent structures at specific sites, and initially, to provide boundary inputs for the numerical models. The surface signatures of coherent structures in the same region will be detected using remote sensing techniques and compared with the *in situ* and model results. The numerical models will serve three roles, viz., (1) precursor simulations in which existing bathymetry and assumed regional forcing will allow us to guide the measurement plans, (2) detailed simulations of both the region and specific local areas for comparison to field-determined coherent structures, and (3) simulations to aid in characterizing the mechanisms by which observed coherent structures are formed, to evaluate the sensitivity of these generation mechanisms to variations in forcing, and to predict the surface signature that such structures generate. Results from the *in situ* field observations, remote sensing, and numerical model runs will be synthesized into a classification scheme that includes all observed coherent structures. Predictive scaling relationships will be developed in order to generalize the results from this study to other systems. The result of this integrated approach will be a thorough

investigation of the mechanisms and evolution of coherent structures in rivers and estuaries in order to link their surface expressions to subsurface flow features.

The project participants have been organized into teams identified by the main areas of interest listed above: Remote Sensing: A. Jessup, W. Plant (APL-UW), and K. Edwards (APL-UW); Modeling: R. Street and O. Fringer (Stanford); In situ Measurements: S. Monismith and D. Fong (Stanford); Physics and Classification: A. Horner-Devine and P. MacCready (UW-Oceanography).

Collaborators that participated in the 2006 field experiment were T. Donato (NRL), who made airborne hyperspectral measurements, and R. Geyer and J. Trowbridge (WHOI), who made subsurface turbulence measurements from the a surface vessel.

Figure 2. Instrumentation barge left) showing infrared and microwave sensors mounted on a hydraulic lift to a height of 28 m above the surface. View from barge (right) showing tip of Jetty Island (near) and rocky sill (far) exposed at low tide. The orange markers mounted on poles were used for georeferencing imagery.

WORK COMPLETED TO DATE

The acronym COHSTREX was chosen for the project, which stands for COHerent STructures in Rivers and Estuaries eXperiment. The focus of experimental work for this reporting period was preparation for and execution of the first major experiment that took place from 3-27 July 2006. Progress was also made in the numerical modeling effort, which contributed to the planning of the field experiment. The location of the experiment on the Snohomish River in Everett, WA is shown in the aerial photographs in Figure 1. The photograph on the right shows the location instrumentation barge and the submerged rocky sill that is exposed at low tide and forms a gap with the north tip of Jetty Island through which the river flows. Figure 2 shows the deployment of IR and video cameras and the RiverScat scatterometer from an aerial lift on a spud barge positioned at the north tip of Jetty Island. This report will highlight progress in the following areas:

- In Situ Measurements: Moorings, 30-hour survey, REMUS (Stanford)
- Physics and Classification of Coherent Structures: Biosonics/ADCP (UW Civil Eng.)
- Infrared Remote Sensing: barge and airborne (UW, APL)
- Microwave Remote Sensing: shore and airborne (UW, APL)
- Numerical Modeling (Stanford)

RESULTS

Processing of the data from the main experiment is underway and promises to provide significant insight into the river flow and the wide variety of coherent structures. Here we provide an overview of the preliminary results to date.

In situ, field measurements

During the past year, our primary focus has been on planning and preparing for the major field experiment With a significant effort on the part of all parties involved at the University Washington and Stanford University, in addition to cooperation with colleagues from Woods Hole Oceanographic Institution, we had an extremely successful experiment with approximately ~95% data recovery for all in situ instrumentation. The analysis of the large datasets will be the primary focus in the upcoming year. The collected data should prove useful for the modeling effort as well as provide important details of the hydrodynamic setting under which the coherent structure fields were observed.

In order to adequately quantify the hydrodynamics dominate the complex Snohomish estuarine system, we expanded our originally proposed experimental setup to include nearly twice the instrumentation in the region of expected coherent structure generation. These additional instruments were obtained by leveraging matching funds with internal funding within Stanford's School of Engineering and also borrowing instrumentation from other field projects at Stanford's Environmental Fluid Mechanics Lab.

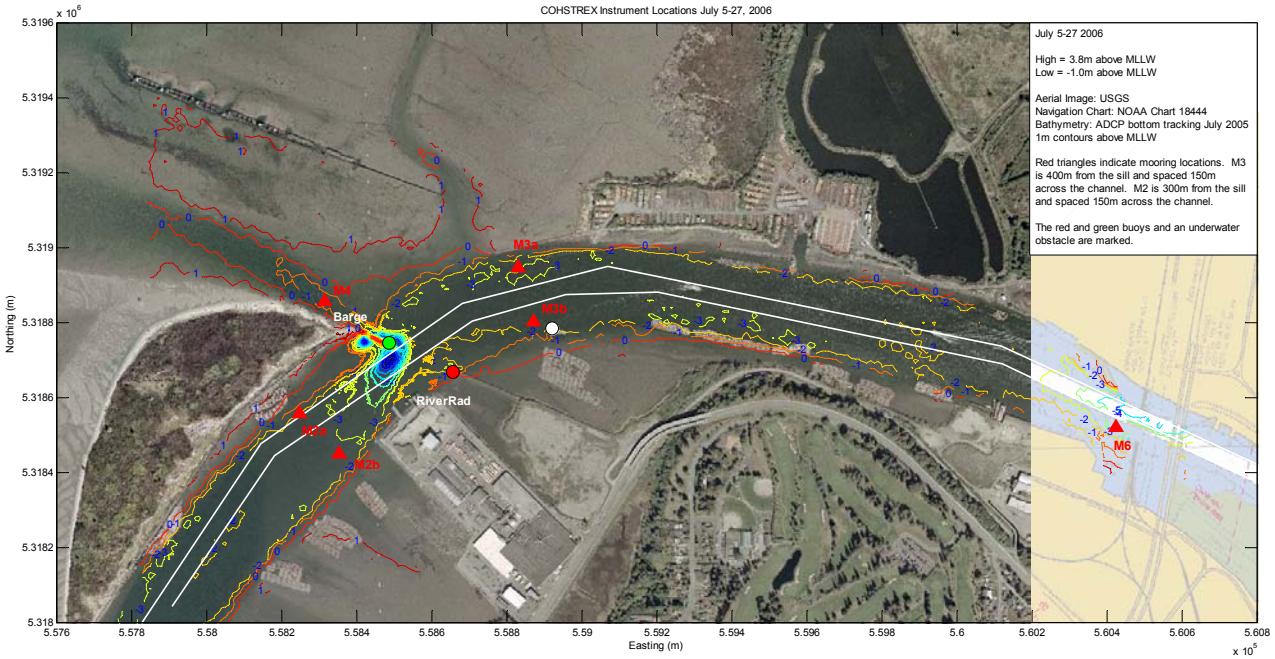

Figure 3: Summary of locations of in situ instrumentation for July 2006 experiment. Aerial photograph with superimposed bathymetry showing the location of the moorings (red triangles).

In order to resolve the cross-channel current variability and turbulence fields, two pairs of high resolution, fast pinging ADCPs, along with surface and bottom mounted CTDs and a nearbed high frequency Acoustic Doppler Velocimeter (ADV) were deployed at two river cross sections surrounding the area of focus for measuring coherent structures (Figure 3). In addition, we deployed additional instrumentation to provide boundary condition information for the broader reaches of the numerical modeling domain of the Snohomish (M4 and M6 in Figure 3)

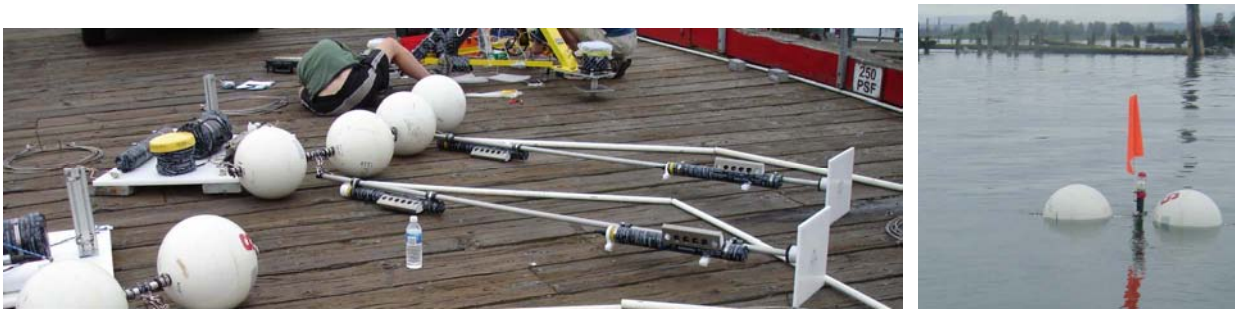

Figure 4: Vertical CTD mounts ready for deployment (7/5/2006—left panel). M3A CTD buoy in place with additional flag and light for visibility (right panel).

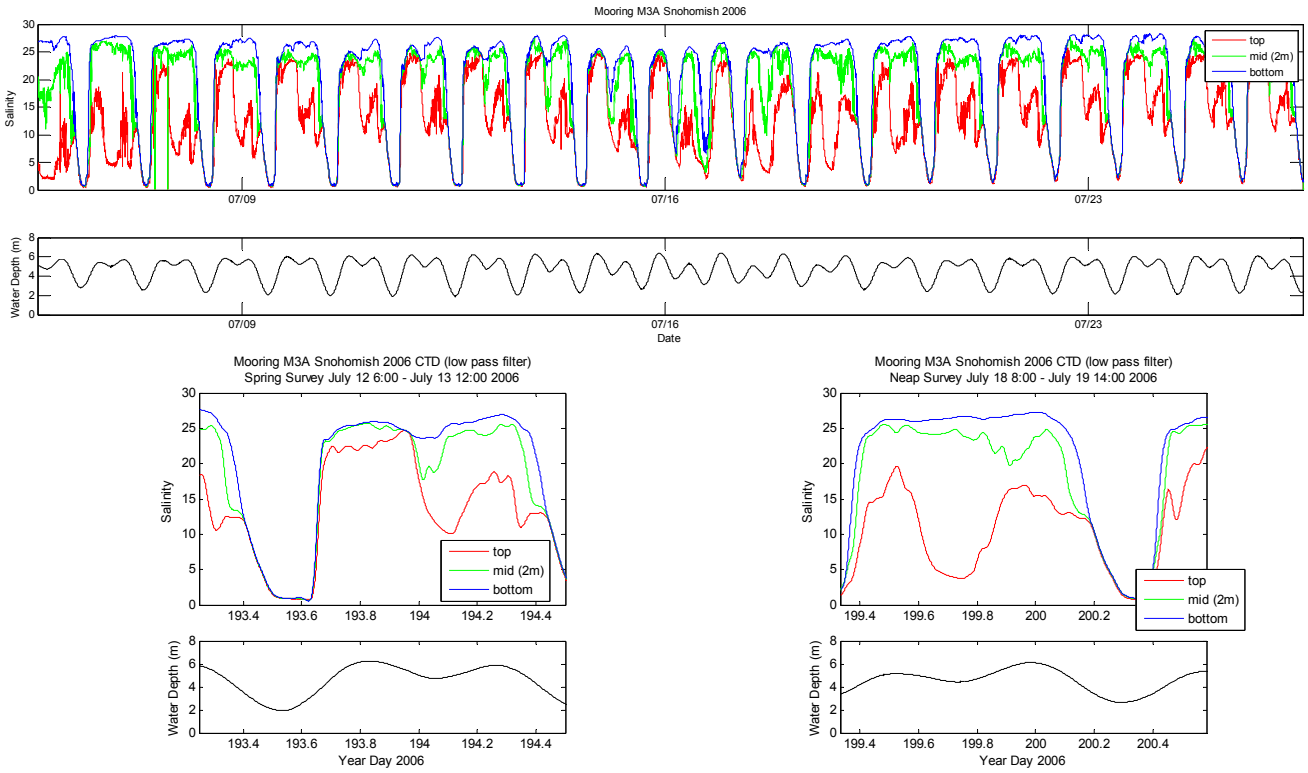

Figure 5. CTD time series, mooring M3A (low pass filtered 1 minute data). Entire records shown in upper panel and subsets for representative spring and neap tides are shown in the lower panels.

A significant amount of effort was put into the design the moorings. For example, we needed to design a mooring that allowed measurement of the density over the entire tidal range, yet protected the instruments (in particular the CTDs) from damage from pumping in air or sediment, and maintaining horizontal position without the surface instrumentation being submerged in the presence of significant currents (over 2 m/s in some locations). The final design is shown in Figure 4. Using proper floatation and a tidally-adjusting mooring system for the mid-water depth and surface CTDs we were able to measure density as at multiple depths with great temporal resolution (Figure 5).

All of the fixed mooring data from the experiment has been downloaded, backed up, and assessed initially for quality. The quality of the in situ data looks excellent and with the exception of some minor instrument malfunctions, the data return was extremely high.

The velocity data from the ADCPs is also of very high quality. The mean time series recorded by the ADCPs show the strong semi-diurnal tidal signal as well as the spring-neap variability (Figure 6). We expect to soon analyze the single ping data collected from all four of the fast sampling ADCPs to compute Reynolds stresses and assess the turbulence levels as a function of time, depth, and cross-channel location (see recent work of Nidzieko, et al., 2006 for the methodologies that will be employed). We will compare these profiles of stress with that derived by the near bed ADVs to form a complete water column profile of turbulence and be able to quantify the bottom roughness and drag in the estuary system both upstream and downstream of the region of interest for the coherent structures as well as quantify any cross-stream variability and temporal variability that may exist.

High resolution spatial maps of velocity and density were also captured during two 30 hour experiments within the one month experiment. Considerable effort will be made in the upcoming year to process the large velocity dataset into a useable form which maps the velocity evolution at fixed spatial slices over the evolving tidal cycles in the region of focus as well as phase adjusting the density (i.e., salinity and temperature profiles from the along estuary CTD casts) information in time to create synoptic snapshots of along-estuary density.

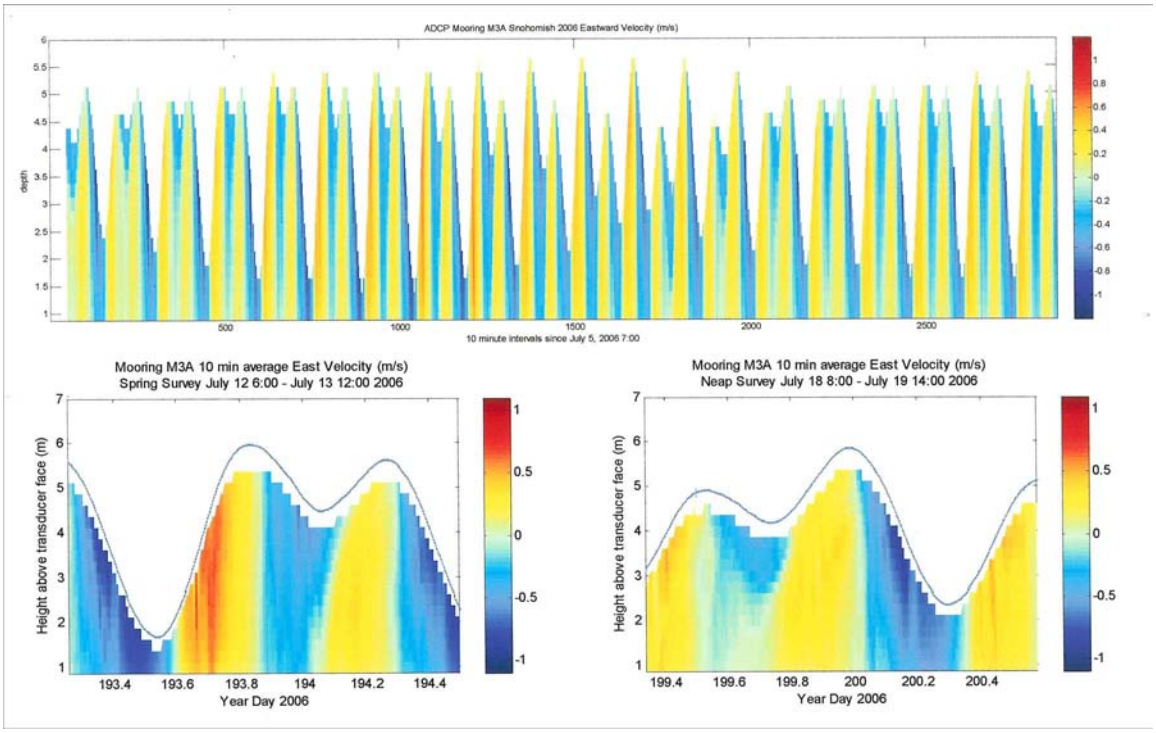

Figure 6. ADCP time series (10 minute averaged) collected at mooring M3A. Entire record shown in upper panel and representative spring neap cycles shown in lower panels.

Finally, we successfully deployed the REMUS autonomous underwater vehicle (AUV) to measure both salinity and temperature variability as a function of space and to evaluate benthic structure and bedforms using its sidescan sonar (Figure 7). Both large features and fine scale bed features are resolved in detail as sand waves ~10 cm high are resolved as well as larger features such as sunken logs. To our knowledge, this is the first use of the REMUS AUV in a shallow, highly energetic tidal system. While the measurements weren't without difficulty, we were able to capture some of the spatial variability in the density field (including part of the salt wedge evolution) as well as map the bottom in great detail. These measurements will be useful in understanding the bottom conditions leading to the turbulent field measured as well as providing feedback to the REMUS development team and AUV community at large on the limitations that must be overcome in order for AUVs to be successfully deployed as the primary hydrodynamics measurement method in such challenging environments.

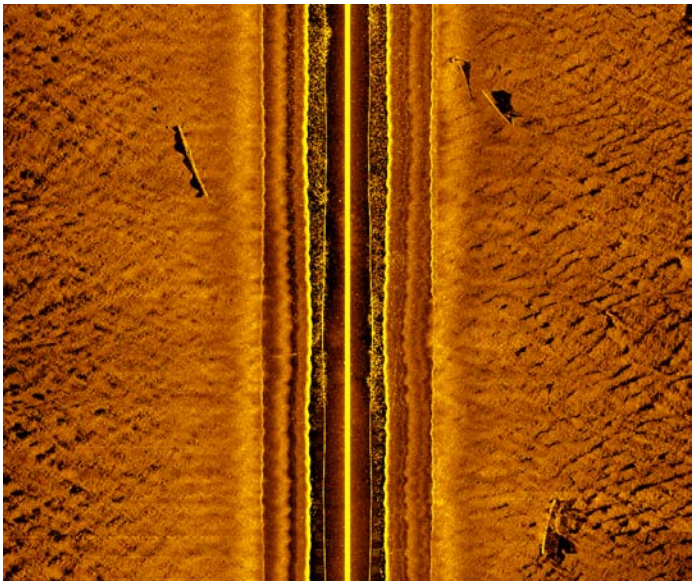

Figure 7. Sidescan sonar image near M3A and the navigation channel (7/17/06). Sand waves ~ 10cm high and logs are clearly visible in this individual image.

In summary, the in situ field measurements were very successful. The datasets collected should provide a detailed look at the hydrodynamics at the field site and be invaluable to better understanding and characterization coherent structures and provide relevant and valuable information for the numerical modeling efforts.

Physics and classification of coherent structures

The in situ observational effort that was focused on the generation of coherent structures involved two measurement platforms (Figure 8). The first consisted of ADCP and CTD boat transects in the region immediately upstream and downstream of the sill. The second consisted of ADCP and acoustic backscatter measurements from a set of tripod-mounted upward-looking instruments located immediately downstream of the sill.

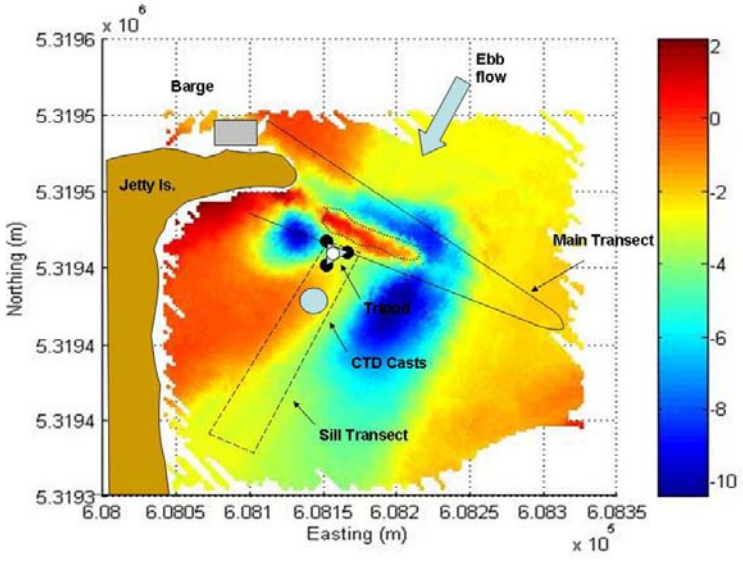

Figure 8: Bathymetric map of the study site showing the location of ADCP transects, CTD casts and the Biosonics/ADCP tripod.

As in the 2005 study, the main sill-parallel ADCP transects capture the structure of the flow incident on the sill. They were repeated two to three times per hour throughout the spring and neap 30 hr studies. A circuit was also sampled downstream of the sill (labeled Sill transect in Figure 8) during the major ebb period of one tidal cycle in order to observe the reattachment of the flow with the bottom. The flow is very complex in this region and it is hoped that these transects will help to understand the details of the flow in which the coherent structures propagate. The data will help with interpretation of the remote sensing data as well as to connect measurements near the sill with measurements made by Geyer and Trowbridge (WHOI) using the MAST further downstream of the sill. Finally, CTD casts were made during a separate ebb cycle in the region immediately downstream of the sill in order to determine the density stratification. The surface velocity in this region during ebb is high so that the boat drifted 10-20 m during one cast. Nonetheless, the data will provide a reasonable measure of the average vertical stratification in the region of boil production.

The tripod configuration included three Biosonics echosounders for imaging the subsurface signature of coherent structures located within the field of view of the remote sensing platform. The exact location of the Biosonics transducers was marked with surface floats and imaged with the remote sensing platform so that the two data sets can be exactly compared. At this point, however, the geo-referencing is still underway and such a comparison can not be made. A 1200 kHz ADCP was also included on the tripod to measure the advection speed of the structures. Although this method for imaging the structures was somewhat experimental, it turned out to be very successful. Typically, one transducer was used at a time and sampled at 25Hz. We observed structures in the top 1-2 m of the water column clearly in the return (Figure 9a) at times when structures were also observed on the water surface. We also observed that the core of the structures contained low-return water at times when cold boils were observed in the infra-red imaging. Since the underlying fluid is generally characterized by lower acoustic return than the surface fluid, we are hopeful that we will be able to differentiate between cold and warm boils based on the Biosonics data. This hypothesis will be tested once the location of the Biosonics beams in the IR field of view has been determined.

Previous studies suggest that the frequency of the boils will depend on the flow speed and flow depth according to a Strouhal relationship. When boils begin to appear the flow is roughly 1 m/s and the water depth above the sill is 1 m, which predict a frequency of approximately 0.1-0.2 Hz. Spectral analysis of the near-surface return from the Biosonics transducer shows that the frequency associated with the boils varies between 0.1 and 0.5 Hz over the course of the ebb (Figure 9b and 9c). By using the Biosonics to determine the exact water depth and the ADCP to determine the mean surface velocity at each time, we will test the above scaling in order to explain the observed variation in boil frequency.

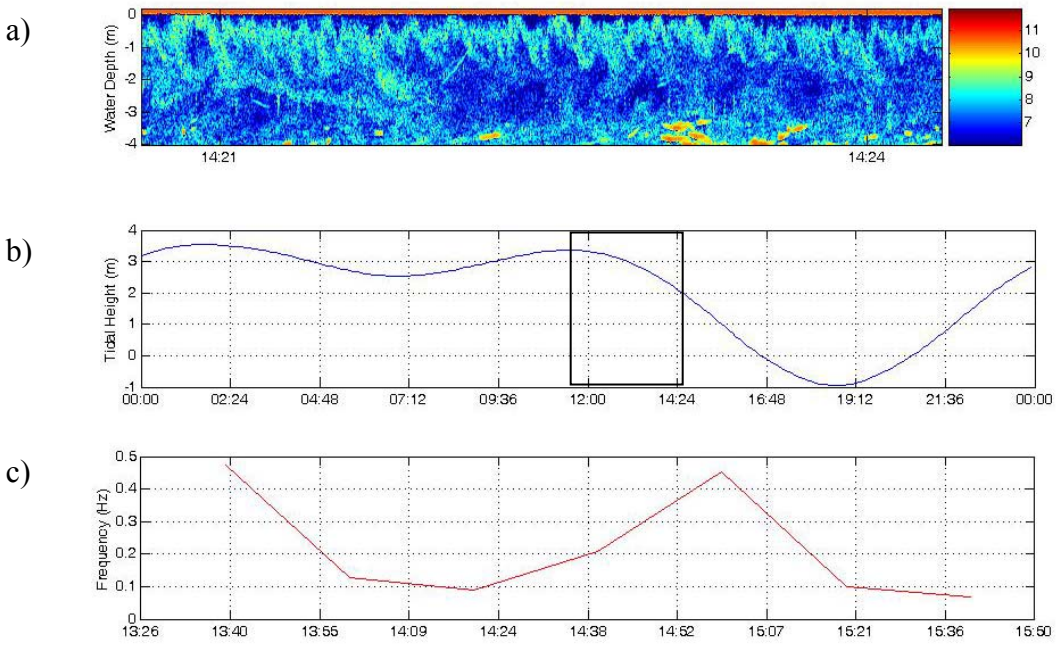

Figure 9: a) Acoustic backscatter intensity from the Biosonics transducer during a period of active boil production. The return is plotted on a log scale and dark blue corresponds to the lowest return. b) Tidal height from the NOAA Seattle gauge during the measurement period in question. The black box indicates the intense boil production period. c) Boil frequencies based on spectral analysis of the near-surface acoustic backscatter during the intense boil production period.

Infrared Measurement

The preliminary experiment in 2005 showed that the occurrence and appearance of coherent structures in the river are highly dependent on the tidal forcing. Furthermore, the nature of the coherent structures varies over relatively large areas because of the variable bathymetry and geometry of the river. Therefore, the primary requirements for remote sensing in this application are the ability to gather long time series of images over a wide area. During the 2006 COHSTREX deployment, stationary measurements from the lift on the barge provided the long dwell time and aircraft-based measurements provided the large area coverage.

A tentative finding from the 2005 preliminary experiment was that the temperature of the boils generated by flow over the submerged sill is determined by the presence or absence of the tidally-driven salt wedge. Validation of this result was a primary focus of the long time series coverage provided by the barge-based measurements. A new image acquisition system was designed to acquire continuous measurement for several hours at a time during ebb and flood tide. In addition to the remote sensing instruments, we deployed CTD sensors on a mooring with cable connections back to the barge. These data provide stratification information in real-time so that we could correlate changes in the boil temperature with the location of the salt wedge. The time series of temperature, salinity, and pressure in Figure 10 show the typical behavior associated with the passage of the salt wedge on both ebb and flood tide.

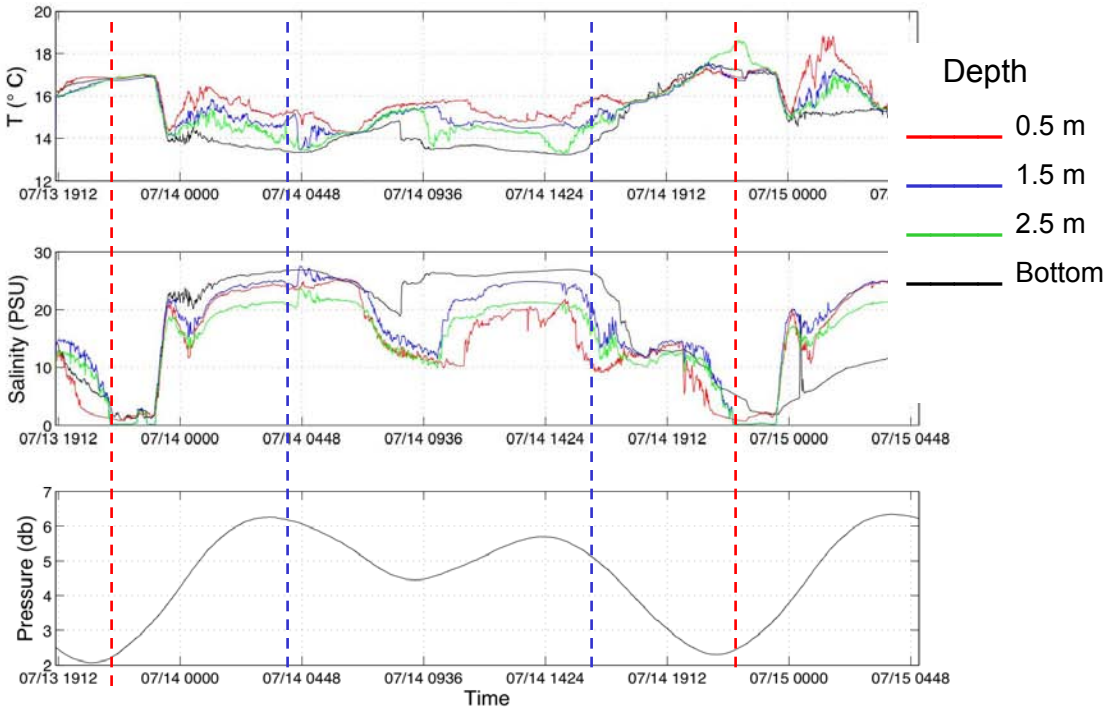

Figure 10. Time series of temperature (T, top), salinity (S, middle), and pressure (bottom) from a mooring approximately 40 m upriver from the sill. The red lines indicate times when the salt wedge was traveling upstream on flood tide, showing an abrupt drop in T and rise in S, followed by stratification. The blue lines indicate times when the salt wedge was traveling downstream on ebb tide, when T increases, S decreases, and both become uniform with depth.

The 2006 measurements confirm the hypothesis that the thermal signature of the boils is determined by the vertical stratification. Furthermore, we found that the boils were generated by flow over the sill on both ebb and flood tide and that their temperature changed accordingly. (The 2005 measurements focused on flood tide, so the ebb tide finding is new.) The three images in Figure 11 span a period of about 40 minutes during ebb tide during which the temperature of the boils changed from cool to warm, corresponding to the passage of the salt wedge downstream. The time series of T, S, and D in Figure 12 cover this period and confirm the correlation.

The area-extensive coverage provided by the aircraft measurements show that the cold signature of the boils persists well downstream of the generation site. Figure 13 compares coincident images from the aircraft and barge at two times, showing how the surface disturbances grow and persist. Finally, Figure 14 shows an example of co-registered event in the aircraft and barge imagery and rectification of the barge imager.

Our preliminary analysis has confirmed that the salt wedge can be detected from the boil temperature. We successfully combined airborne surveys and fixed time series to produce a high quality data set that is rich in variety of coherent structures.

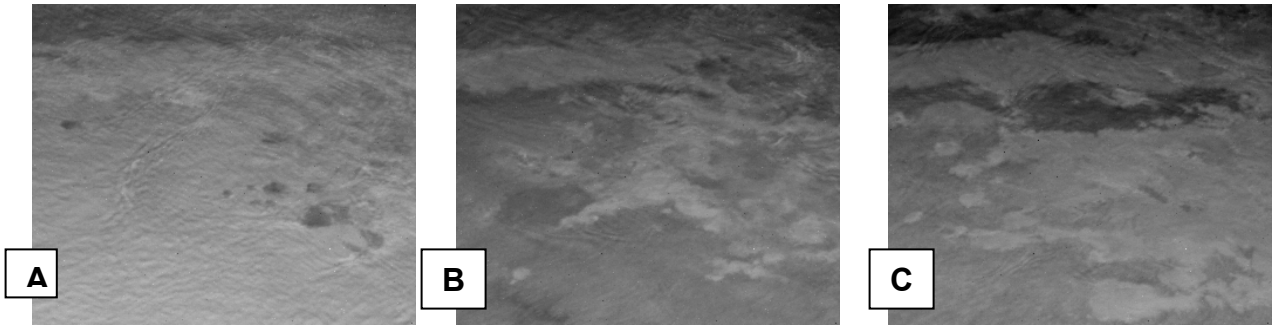

Figure 11. Sequence IR images of boil field generated downstream of submerged sill during ebb tide (lighter grey is warmer). The images are labeled A-C and correspond to the times indicated by letter in the time series of T, S, and D in Figure 12. At time A, the vertical stratification is strong enough that the boils appear cool because they bring up colder water from the bottom. By time C, the stratification has weaked to the point where the boils appear warm because they are disrupting the cool skin.

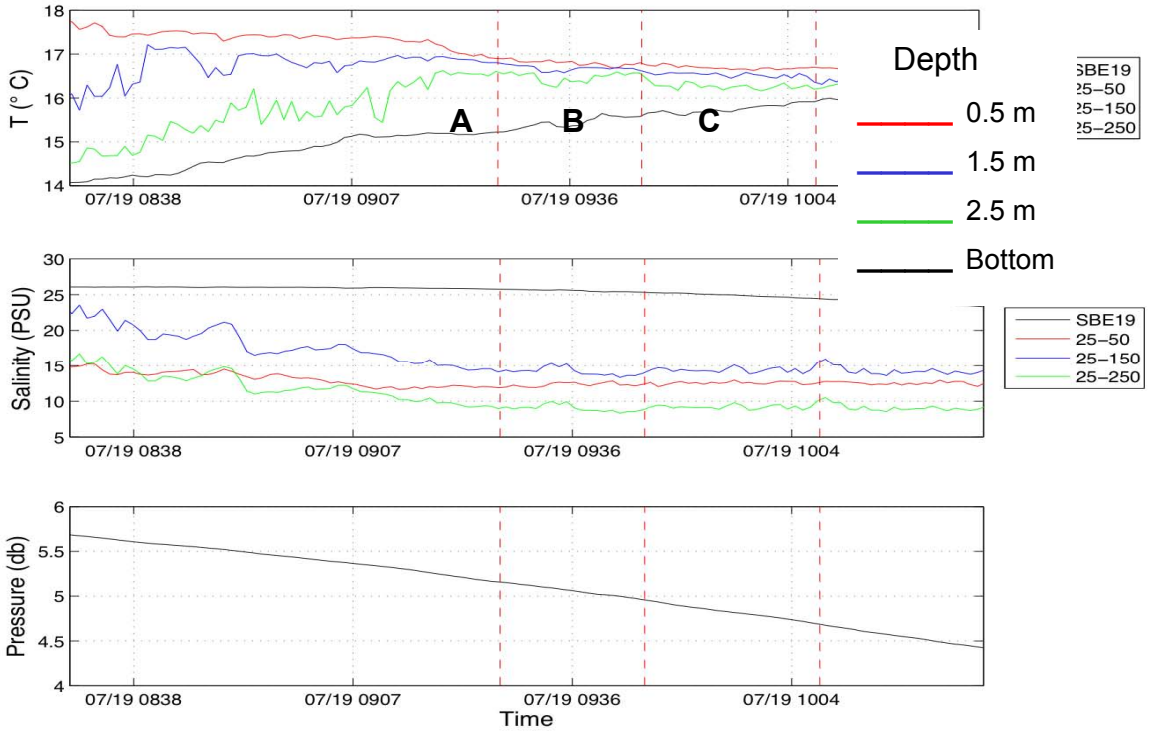

Figure 12. Time series of T, S, and D covering the period of the images in Figure 11. The times A-C correspond to the images in Figure 11.

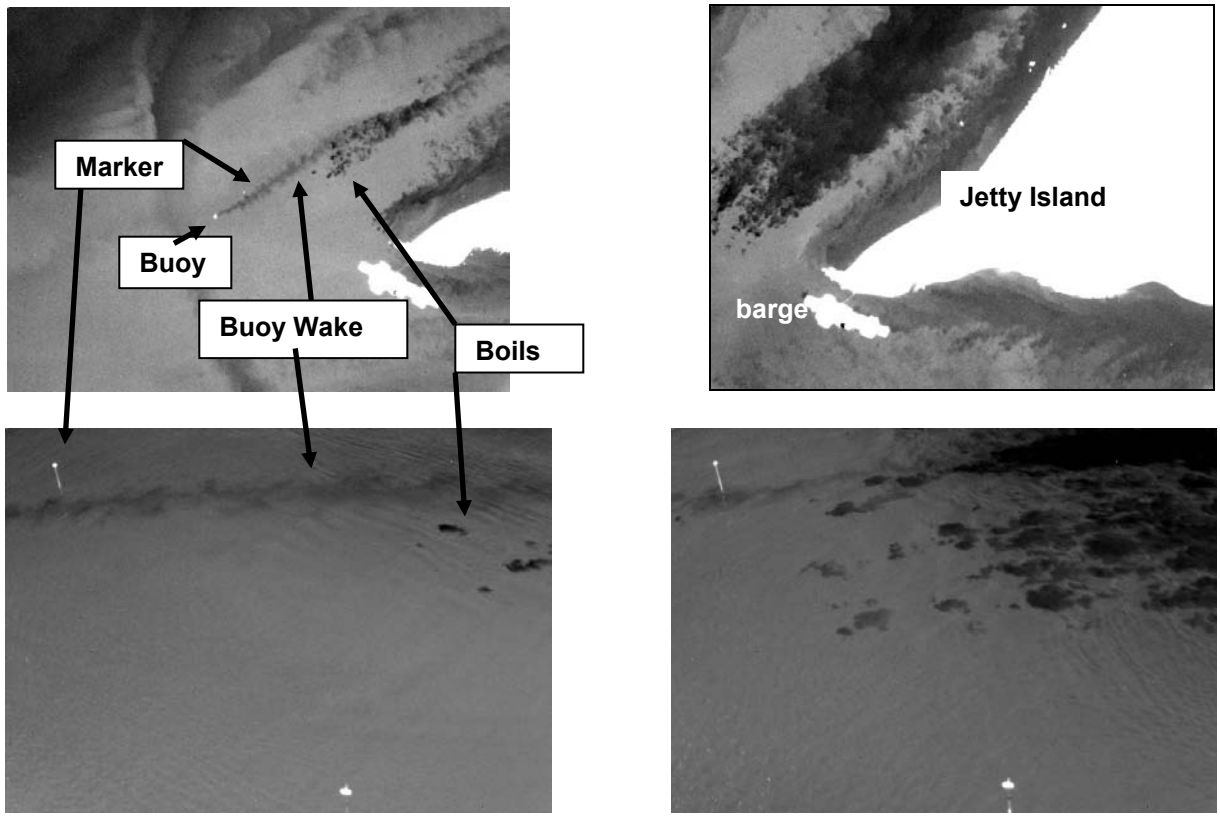

Figure 13. Comparison of coincident IR imagery of evolving boil field from aircraft (top) and barge (bottom) during ebb tide. The right images were taken 45 minutes later than the left. The same individual boils can be identified in both the airborne and barge-based images. The airborne images show the downstream growth and persistence of the surface disruptions.

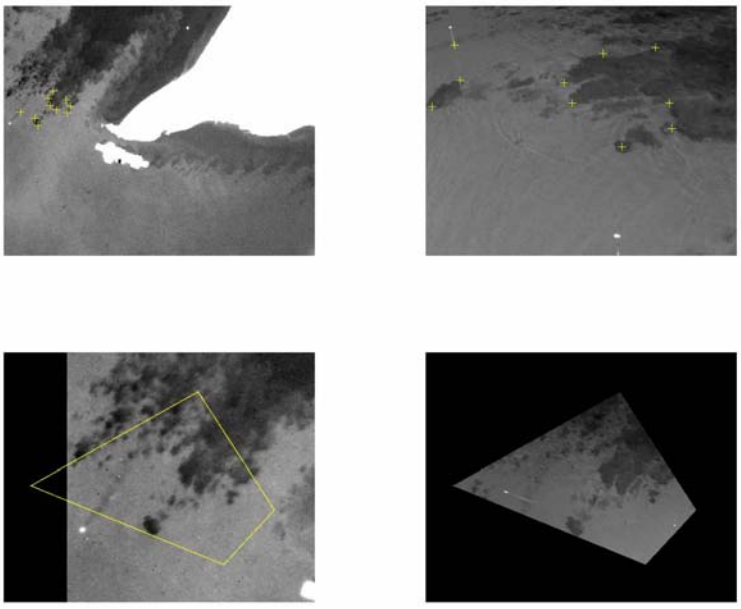

Figure 14. Co-registration of features and image rectification. Top row compares airborne (left) and barge (right) with a number of features marked (+) in both views. The barge-based image in the bottom row (right) has been rectified and its outline is shown in the magnified aerial image (bottom left).

Microwave Remote Sensing

In July, 2005, our group deployed our continuous-wave Riverscat system on the barge alongside Andy Jessup's IR instruments. We also deployed our pulsed Doppler radar, RiverRad after some modifications, at the Rinker's Asphalt Plant across the Snohomish River from the tip of Jetty Island. In July, 2006, we deployed these same two instruments in the same locations and also flew our CORAR airborne Doppler radar on a DeHavilland Beaver rented from Kenmore Air.

Analysis of Riverscat output in the form of Doppler spectra and currents is in the process of being compared with currents measured from the IR imagery.

RiverRad data from 2005 have been converted to imagery and have shown several interesting features in the flow patterns of the Snohomish River at various stages of the tidal cycle. Examples are displayed in Figures 15-17.

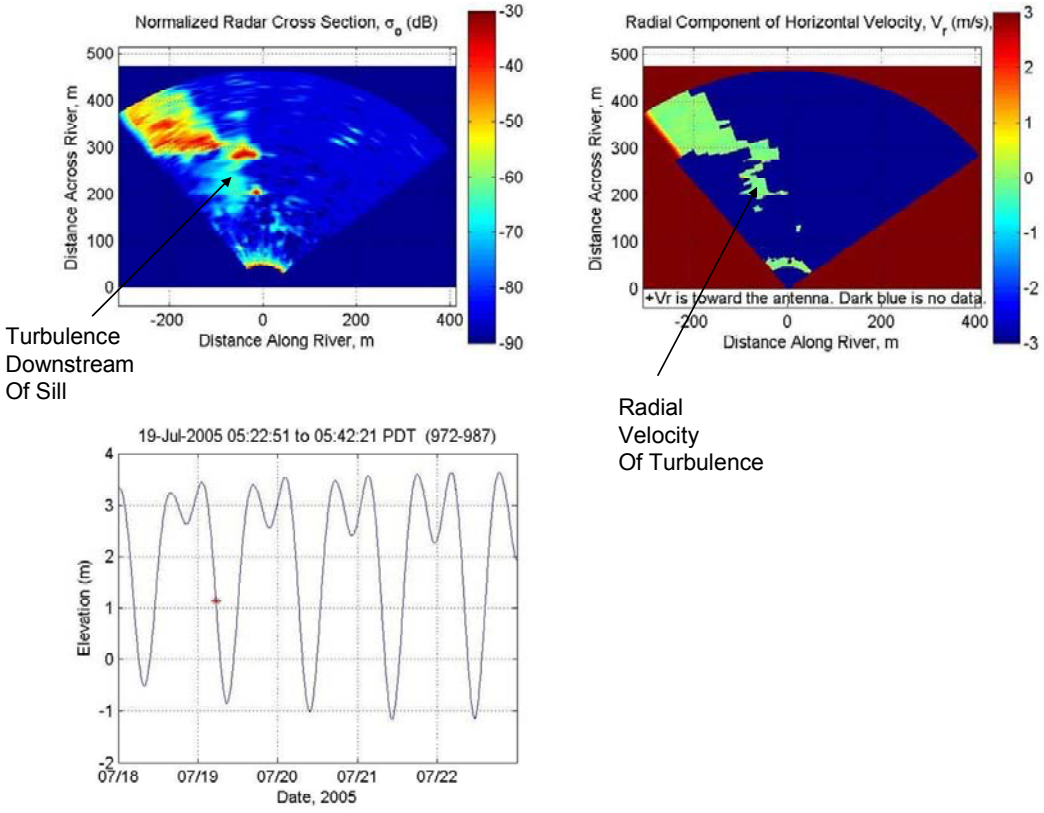

Figure 15. Turbulence downstream of the sill at the north end of Jetty Island. The red dot in the lower left plot shows the phase of the tide when the image was collected.

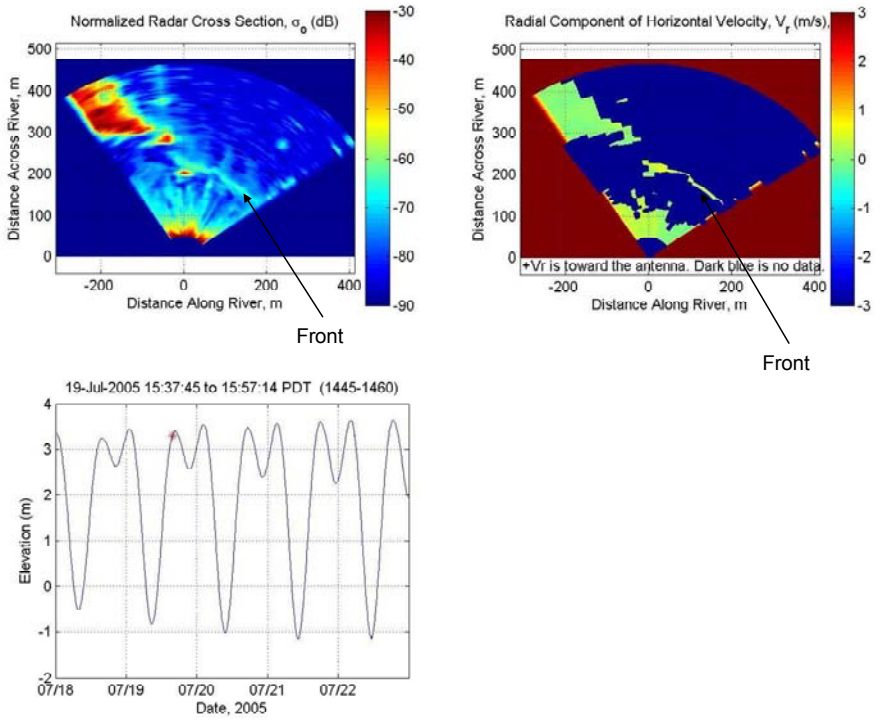

Figure 16. Increased radar backscatter at the front between the main channel water and water from the overflow channel.

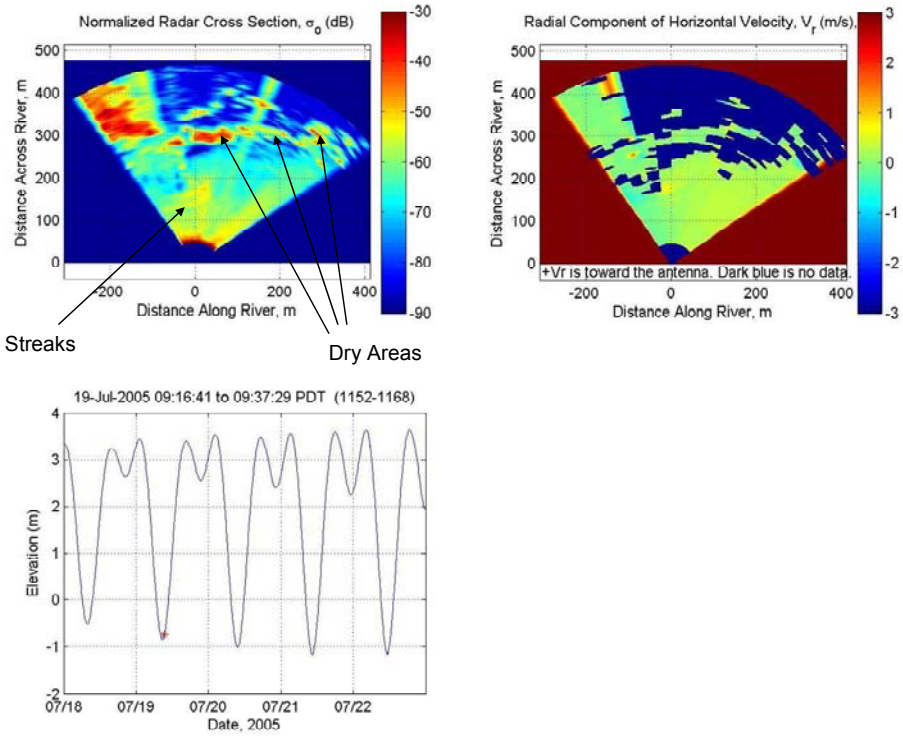

Figure 17. Two parallel streaks of enhanced backscatter at low tide. Possibly associated with the dredged channel.

Figure 18 shows an overview of the study site and RiverRad deployed at the asphalt factory in 2006.

Figure 18. Photo (right) of the site of the COSHTREX measurements taken from the beaver. The barge with the IR and microwave equipment is in the lower center just off the north tip of Jetty Island. The sill was exposed at this time. The ship in the channel contains the WHOI equipment. RiverRad was set up just off the picture to the left of the pilings seen in the top left. The photo on the right shows RiverRad deployed at the asphalt factory in 2006.

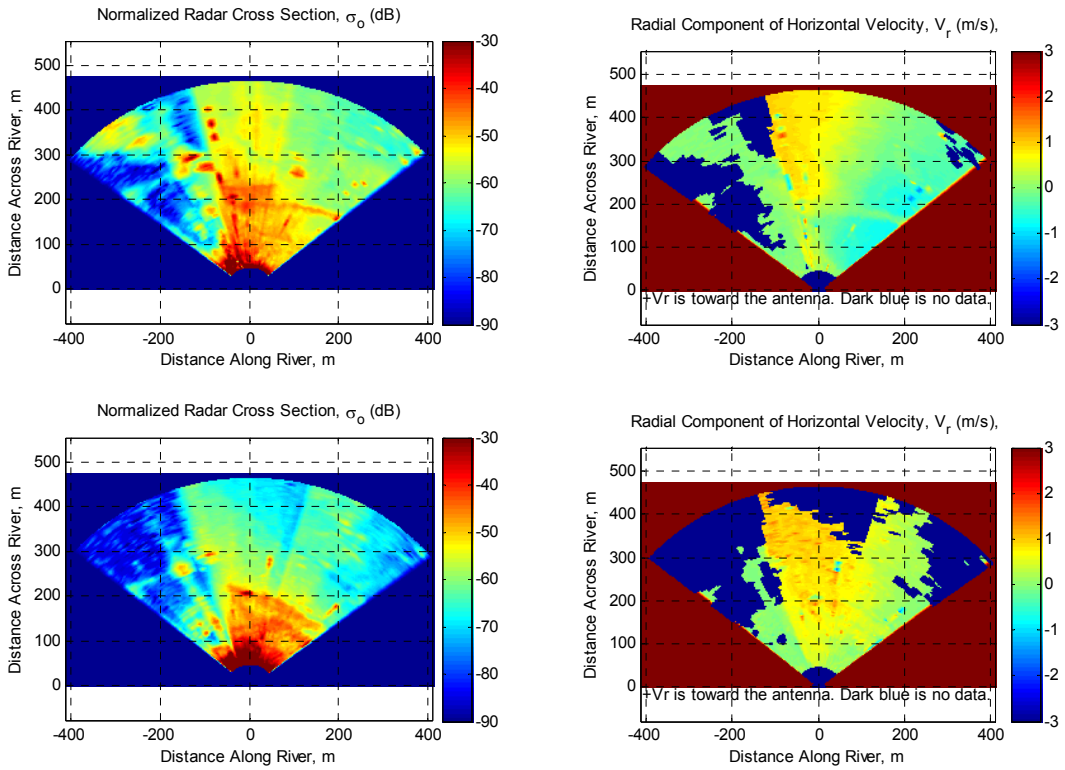

Figure 19. Images from the RiverRad 2006 deployment. Left are cross sections, right are the corresponding radial velocities.

Figure 20 shows CORAR as deployed on the Beaver in 2006.

Figure 20. CORAR deployed on the DeHavilland Beaver.

Data collected in this year have not all been converted to images yet. An example of some images from data collected early in the experiment is shown in Figure 19 where the dual streaks and/or frontal features seen in 2005 again appear to be present.

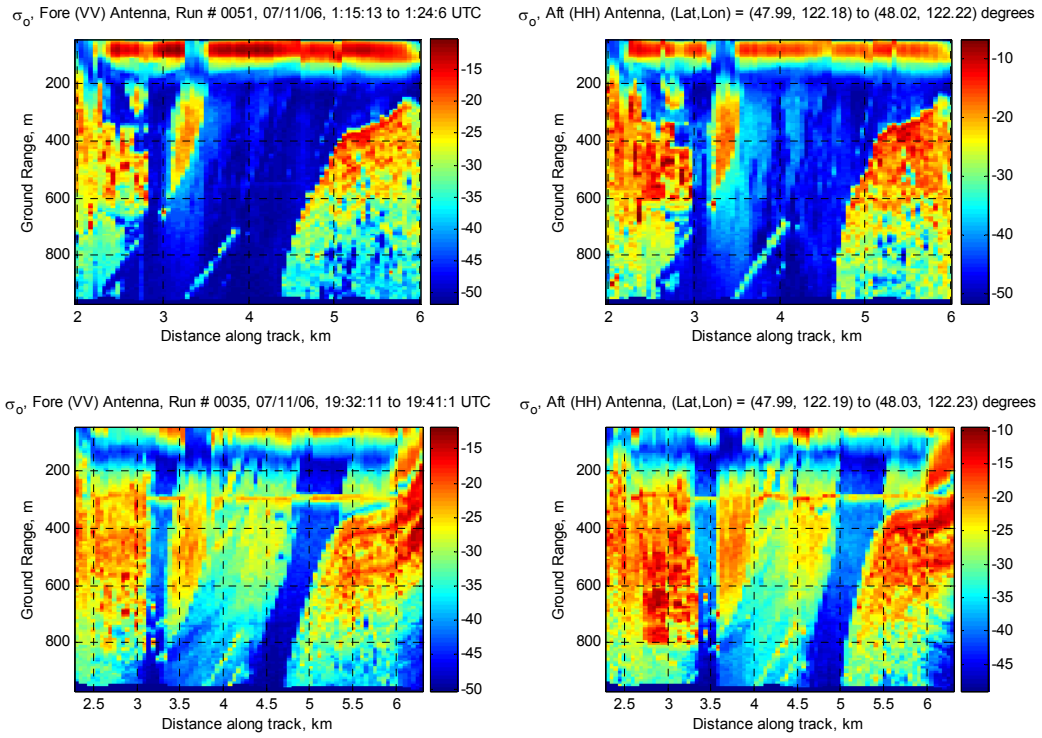

Figure 21. Preliminary cross section images of Jetty Island and the surrounding river taken on July 11, 2006 at two different times. Images on the left are VV polarization. Those on the right are HH. South is up, Jetty Island is at about 3 km along track, and the row of pilings runs from 3.2 to 3.8 km along track and 900 to 700 m in ground range.

On the second day of flights, the microwave power amplifier failed and the flights were terminated. We therefore have data only for July 11, 2006. Images of cross sections at vertical and horizontal polarizations for one of these flights are shown in Figure 21.

Analysis of data from both years is continuing. We want to complete the comparison of Riverscat surface velocities with those from the IR in the near future and compare the features seen in the RiverRad imagery with models after that. We will also process and analyze the single day of CORAR data as completely as possible.

Numerical Modeling

During the past year, we have focused on completing the set-up and early runs with the SUNTANS code. A major effort was aimed at grid generation; also the advection algorithm was changed to an Eulerian-Lagrangian method to facilitate the significant wetting and drying of the coastline during the large Snohomish tidal range.

BACKGROUND AND SETUP

The bathymetry data used in the numerical model is a combination of data measured by Finlayson in 2000, the field measurement data obtained by our team last year in the river channel and mouth, and the field measurement data by Fram (2002), which gives an estimated bottom slope for Snohomish River upstream from the bridge.

In order to capture the interaction between the river and the tide, the computational domain is chosen as shown in Figure 22 to include the Snohomish River Estuary, 30 kilometers of Snohomish River in the east, Possession Sound in the west, and Port Susan (a closed-end bay connected to Possession Sound). Whidbey Basin, another basin connected to Possession Sound, is not in the model. Steamboat Slough as a tributary of the Snohomish River is modeled.

In addition to the closed boundaries for coastlines and river banks, there are three open boundaries, two forced with tides [at the junction of Possession Sound and Whidbey Basin, and at the junction of Possession Sound and Main Puget Sound Basin] and one with Snohomish River flow. Studies by Fram (2002) showed that the salt wedge goes up to 13 km upstream from the river mouth. Because the gage data at USGS Gage Station (Snohomish River at Snohomish), located 20 km from the river mouth, shows significant tidal influence, the grid is extended to 30 km upriver where the next USGS gage station (Snohomish River near Monroe) shows no tide influence.

An unstructured grid of 36,000 horizontal cells has been generated with GAMBIT. This grid has 600m resolution for Puget Sound and 80m resolution for the river channels. Cells with 20m resolution are used at the focus site [Jetty Island]. This grid is sufficient for capturing the main flow conditions, but not for resolving fine coherent structure detail. It has been found efficient and useful in the initial testing.

We have a grid that has been further refined at the focus site (Figure 23). It has 300m resolution for Puget Sound, 80m resolution for the river and 1m resolution for the coherent structures. It consists of 100,000 horizontal cells. We are currently working on improving the quality of this grid for production computations.

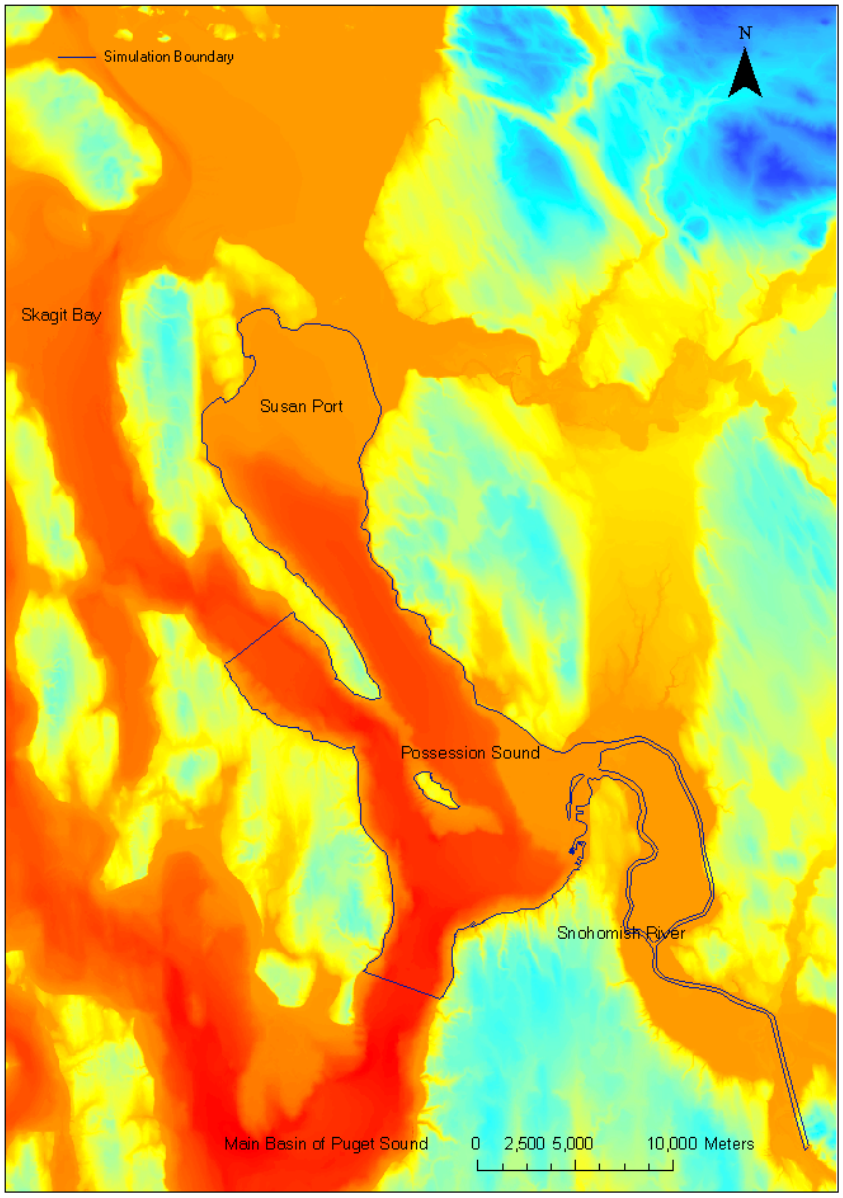

Figure 22. Simulation domain and boundaries.

Observations and studies on the circulation in Puget Sound (Gustafson et al 2000; Stout et al 2001; and Lavell et al 1988) have shown that Possession Sound, Port Susan and Whidbey Basin act like a closed basin and that the depth in entire area varies at the same pace (in phase). Thus, fluxes through a specific cross section can be estimated via volume conservation and forcing done with the expected tidal values. The results are in agreement with the predictions from Lavelle's model.

There are three river flows, viz., the Skagit River, the Snohomish River and Stillaguamish River [but the latter is a minor contributor and is ignored]. The discharge rates of the rivers are found in USGS databases and a few other documents. The Skagit River is not modeled, but its freshwater inflow enters our computational domain through the north tidally-forced boundary, and then goes out through the south boundary. The water from the Snohomish River comes in through the river inlet and flows out through the south boundary.

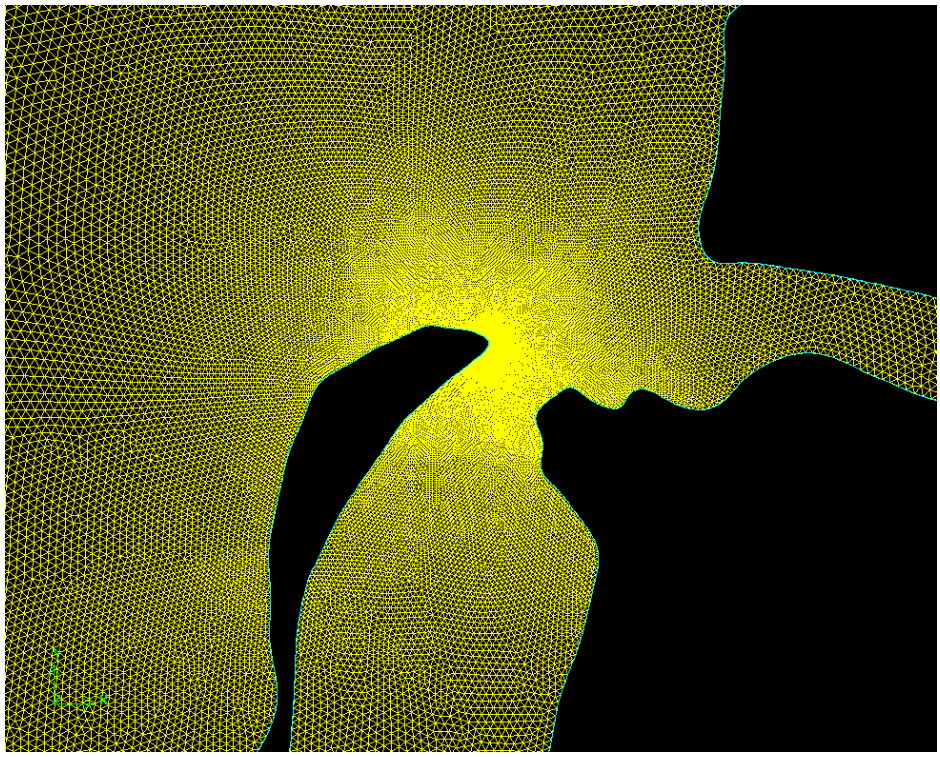

Figure 23. The focus site on the fine grid

The saline water in the sound is slightly stratified, with the typical salinity of 27 psu or so near the top (Gustafson, 2000). In our simulation, we assume that the flows in and out of the tidally forced boundaries are saline water of 30 psu, and the river inflow is 0 psu. The simulation starts from quiescent conditions at HHW. As Fram (2002) found that the salt wedge travels up 10km from the river mouth at HHW, we setup the initial conditions with a linear horizontal salinity gradient changing from 30psu to 0psu at that location. Water downstream of that is saline and upstream of that is fresh.

SIMULATION RESULTS

Multiple test runs have been performed to improve the boundary conditions and drag coefficients. The following results from the recent runs are an illustration of the simulations. These runs are hydrostatic without a turbulence mixing model. However, they have modeled the nonlinear advection of momentum under wetting and drying conditions. The predicted free surface height matches the real tide pattern reasonably well in most of the deeper Possession Sound areas. The prediction near Jetty Island shows a lag at low low water, which is reasonable. It has underestimated the amplitude of the ebb a bit. Further upstream at the USGS Gaging Station there is a similar underestimation of the ebb. River slope and bottom drag are being investigated as possible causes of this behavior.

Figure 24 shows velocity fields near the free surface at low low water and on a strong flood tide. The model is able to capture a number of observed features of the real flow: (a) the significant drying that happens at low low water, when only the deepest part of the bypass to the north of Jetty Island stays wet; (b) flow is strong during ebb; (c) at high high water, the currents are very slow.

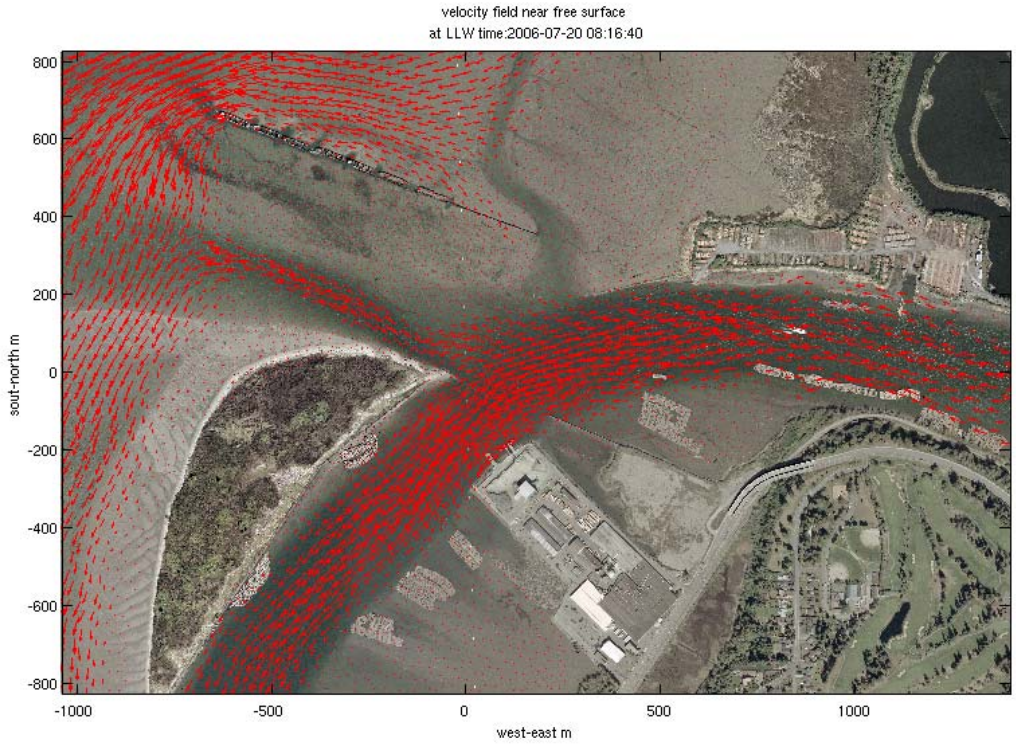

Figure 24(a). Velocity field at LLW on July 20th

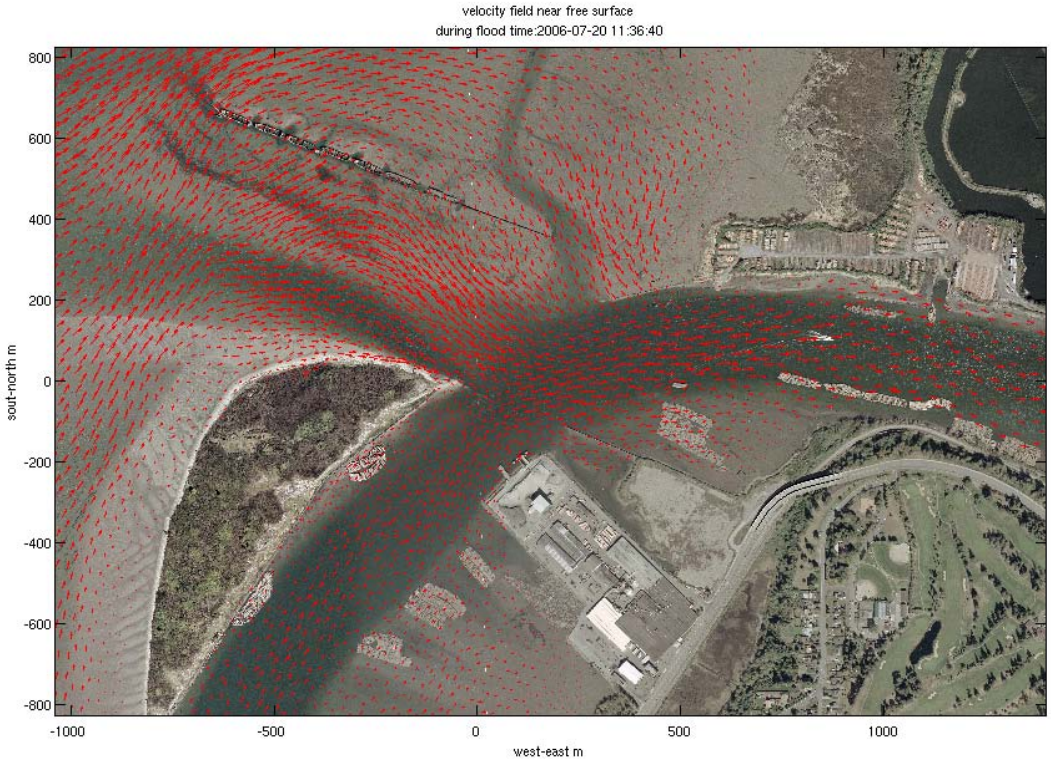

Figure 24(b). Velocity field during strong flooding

IMPACT/APPLICATIONS

Our results demonstrate how currently available prediction schemes and observing systems (remote sensing and AUVs) can be combined for operational applications.

RELATED PROJECTS

None to date.

REFERENCES

Fram, P.J., et al. (2002). Longitudinal and Lateral Salt Gradients of the Snohomish River Estuary: Summer Research Project at Friday Harbor Laboratories. Poster.

Gustafson, R.G., W.H. Lenarz B.B. McCain, C.C. Schmitt, W.S. Grant, T.L. Builder, and R.D. Methot. (2000). Status review of Pacific Hake, Pacific Cod, and Walleye Pollock from Puget Sound, Washington. U.S. Dept. Commer., NOAA Tech. Memo. NMFS-NWFSC-44, 275p

Lavelle, J. W., H. O. Mofjeld, et al. (1988). A multiply-connected channel model of tides and tidal currents in Puget Sound, Washington and a comparison with updated observations. Seattle, WA, Pacific Marine Environmental Laboratory: 103.

Nidzieko, N. J., D. A. Fong, and J. L. Hench, 2006. Comparison of Reynolds stress estimates derived from standard and fast-ping ADCPs. *Journal of Atmospheric and Oceanic Technology*, 23 (6): 854-861.

Stout, H.A., R.G. Gustafson, W.H. Lenarz, B.B. McCain, D.M. VanDoornik, T.L. Builder, and R.D. Methot. (2001). Status review of Pacific Herring in Puget Sound, Washington. U.S. Dept. Commer., NOAA Tech. Memo. NMFS-NWFSC- 45, 175 p.